American Mineralogist, Volume 107, pages 1598–1610, 2022

Helvine-danalite mineralogy of the Dulong Sn-Zn polymetallic deposit in southeast Yunnan, China

Shiyu Liu[1], Yuping Liu[2,*], Lin Ye[2,*], Chen Wei[2,3], and Weihong Chen[2,3]

[1]College of Resources and Environmental Engineering, Guizhou University, Guiyang 550025, China
[2]State Key Laboratory of Ore Deposit Geochemistry, Institute of Geochemistry, Chinese Academy of Sciences, Guiyang 550081, China
[3]University of Chinese Academy of Sciences, Beijing 100049, China

Abstract

Southeastern (SE) Yunnan is a major Sn polymetallic province of China, with the Dulong large Sn-Zn polymetallic deposit (in the Laojunshan orefield) being one of the most representative deposits. Our recent work had first identified helvine-group minerals in this deposit. These minerals mainly occur in massive sphalerite ores, and coexist with sphalerite, pyrrhotite, biotite, talc, cassiterite, and fluorite. Raman spectroscopic, X-ray diffraction (XRD), scanning electron microscopic (SEM), and electron probe microanalysis (EPMA) analyses indicate that these helvine-group minerals are oscillatory-zoned helvine-danalite. Both the helvine and danalite zones are mixed with varying proportion of the other helvine-group end-member, and our studies indicate that the oscillatory zoning was formed mainly by periodic fluctuations of the fluid physicochemical conditions (notably f_{S_2} and f_{O_2}), but less related to the variation of the fluid Mn, Fe, and Zn contents. The helvine zone was likely formed in a higher f_{S_2} but lower f_{O_2} environment than the danalite zone. In this study, we present the first LA-ICP-MS in situ trace element data for the helvine-danalite minerals from Dulong, and the results indicate that the helvine has considerably high contents and a wide range of trace elements. The helvine is rich in Ca, Al, Sc, and Y, while the danalite is rich in Sn and P (reaching thousands of parts per million). Such trace element enrichments are likely controlled by their respective ionic size and chalcophile behavior.

Meanwhile, the f_{O_2} and f_{S_2} conditions during the zoning formation may have also influenced the trace element distributions: trace elements may have mainly entered the helvine-group minerals by substituting into the M-sites in $M_4[BeSiO_4]_3S$, for instance Al, Sc, and Y substitute for Mn, and Sn and Mg for Fe and Zn. It is noteworthy that the helvine and danalite zones are all HREE-enriched and have distinct negative Eu anomalies. This may be related to the high fluid F-Y-P contents during the mineral formation. High-F-Y fluids can readily incorporate HREEs into helvine-group minerals, and phosphates incorporate HREEs more readily in alkali fluids. Europium occurs as Eu^{2+} in the fluid, causing the negative Eu anomalies observed. We have also identified grains of cassiterite in the helvine-group minerals and its coexisting sphalerite. U-Pb dating on these cassiterite grains yielded 86.5 ± 1.6 Ma, coeval with the reported sulfide mineralization age. This indicates that both the Be and Sn-Zn polymetallic mineralization occurred in the Cretaceous, and may have been products of the Late Yanshanian Laojunshan magmatic-hydrothermal activity. Considering the close relations with many W(-Be) deposits nearby (e.g., Nanyangtian, Saxi, and Maka), the Laojunshan orefield may also have substantial Be mineralization potential.

Keywords: Helvine-group minerals, physicochemical environment, major and trace element compositions, LA-ICP-MS, cassiterite U-Pb age, Dulong Sn-Zn polymetallic deposits

Introduction

Beryllium is a lithophile rare metal (Goldschmidt 1932), with its upper crustal abundance (~2.1 ppm) being around 30 times its abundance in the primitive mantle (~0.07 ppm) (Taylor and McLennan 1995). Beryllium minerals are commonly found in hydrothermal deposits associated with granitic pegmatites, skarns, and alkaline and (sub-)volcanic rocks. In nature, Be minerals mainly comprise silicates and aluminosilicates, among which beryl, bertrandite, and helvine-group minerals have industry value (Grew and Hazen 2014). Helvine-group minerals are important Be minerals, which have the general formula $M_4[BeSiO_4]_3S$ with M = Mn (helvite), Fe (danalite), or Zn (genthelvite). The crystal structure belongs to sodalite-type, in which the $[SiO_4]$ and $[BeO_4]$ tetrahedra are interlinked into four- or six-membered rings (Hassan and Grundy 1985; Nimis et al. 1996). It is generally considered that helvine is formed in granites or granitic pegmatites, especially in their intrusive contact zones or endoskarns. Danalite is commonly formed in skarn or contact metamorphism-related deposits and granite or pegmatite. Genthelvite is considered to be the rarest helvine-group minerals, and its presence is only documented in calc-alkaline

* Yuping Liu and Lin Ye are the corresponding authors. E-mail: liuyuping@vip.gyig.ac.cn; yelin@vip.gyig.ac.cn. Orcid (L. Ye) 0000-0002-2557-8314

0003-004X/22/0008–1598$05.00/DOI: https://doi.org/10.2138/am-2021-7919

granites, pegmatite, and some contact replacement-type altered rocks (Raade 2020). At present, there are not many studies on the helvine mineralogy in the region, and not much is known about its trace element (including REE) compositions or any petrogenetic link between the helvine-group minerals.

The Laojunshan region in SE Yunnan is an important Be province in China (Li et al. 2017), which hosts the large Nanyangtian beryl gemstone deposit and the small Saxi beryl gemstone deposit/prospect. In recent years, helvine mineralization was discovered at Maka in the northern part of the Laojunshan intrusion (Du et al. 2014). These deposits/prospects are distributed around the Late Yanshanian Laojunshan intrusion (Fig. 1), but there is basically no research on the Be mineralogy in the area, with the Be mineralization age and ore-formation process still under dispute. The Dulong Sn-Zn polymetallic deposit is the largest (superlarge-scale) polymetallic deposit in the district (Fig. 1), and it is widely accepted that its mineralization is closely related to the Laojunshan granite (e.g., Wang et al. 2014; He et al. 2014, 2015; Xu et al. 2015; Ye et al. 2016, 2017, 2018; Zhao et al. 2018). In this paper, we report our first discovery of abundant independent Be minerals (helvine-group) from the deposit. It is noteworthy that some of the helvine-group minerals are euhedral and oscillatory zoned and contain several geochemical indicator elements (e.g., Mn, Fe, Zn) that can provide more information on the SE Yunnan Be ore-formation process and helvine mineralogy. we conducted laser Raman spectroscopy, X-ray diffraction (XRD), backscattered electron (BSE) imaging, electron probe microanalysis (EPMA), and laser ablation-inductively coupled plasma-mass spectrometry (LA-ICP-MS) analysis on the helvine-group minerals from the Dulong orefield, to understand their mineralogy and the physicochemical conditions of the formation of these minerals. We also conducted U-Pb dating on the cassiterite coexisting with Be minerals to unravel the timing of Be mineralization in the Laojunshan orefield.

Geological background

The Dulong ore district is located in the southwestern part of the Laojunshan Metamorphic Core Complex, and situated in tectonic junction between the western end of the Huanan nappes, the Yangtze block, and the Ailaoshan fold belt (Fig. 1a). Exposed stratigraphy in the region comprises mainly the Paleoproterozoic Mengdong Group and Cambrian Xinzhai Formation, Cambrian and Devonian sedimentary rocks, and Silurian Nanwenhe and Cretaceous Laojunshan granites (Fig. 1b). The Paleoproterozoic Mengdong Group is dominated by two-mica (quartz) schist, granulite, and plagioclase amphibolite, which

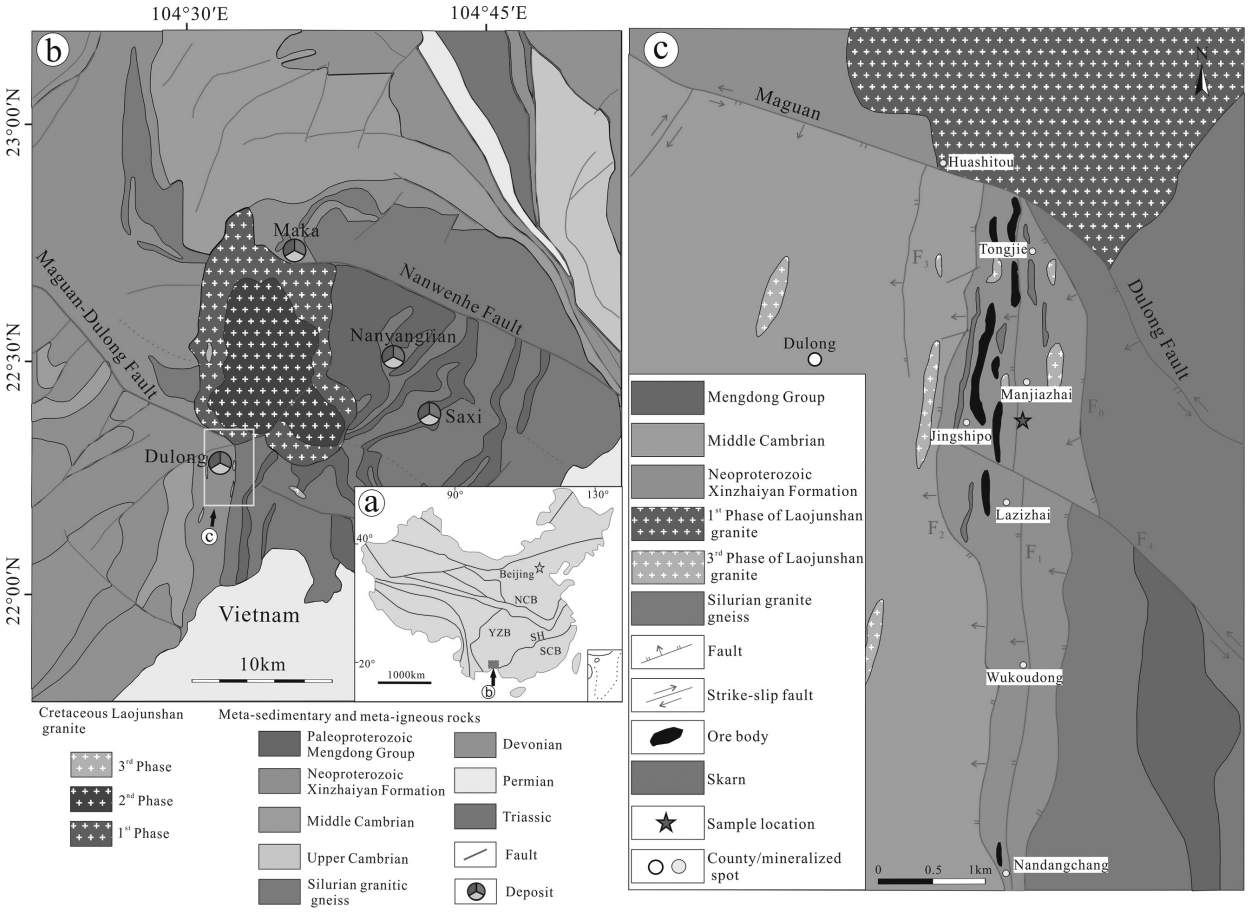

Figure 1. (**a**) Simplified structural map showing the location of the study area. (**b**) Geological sketch map of the Laojunshan Metamorphic Core Complex in SE Yunnan, SW China (modified after Liu et al. 2006). (**c**) Geological map of the Dulong Sn-polymetallic skarn deposit (modified after Liu et al. 2007).

was SHRIMP zircon U-Pb dated to be ca. 761–829 Ma (Liu et al. 2006). The Silurian Nanwenhe granite (SHRIMP zircon U-Pb age: ca. 440–420 Ma; Liu et al. 2006) is exposed in the eastern Dulong, and was metamorphosed/deformed during the Triassic Indosinian orogeny (Yan et al. 2006). The Cretaceous Laojunshan granite is an intrusive complex and comprises (1) medium- to coarse-grained two-mica monzogranite (100–118 Ma) around (2) medium- to fine-grained two-mica monzogranite (90–98 Ma). These rocks were intruded by (3) quartz porphyry and granite porphyry stocks (76–88 Ma) (e.g., Liu et al. 2007; Lan et al. 2016). Previous petrological and geochemical studies indicated that these granite suites are all highly fractionated S-type, and sourced from partial melting of the Mesoproterozoic argillaceous bedrocks. These magmatic suites were likely formed in a back-/intra-arc extensional environment, associated with large-scale lower crustal delamination and asthenospheric upwelling (e.g., Xu et al. 2015; Zhao et al. 2018). Regional faults at Dulong include mainly the northwest (NW) trending Maguan-Doulong and Nanwenhe faults, and a set of northeast (NE) trending secondary faults (Fig. 1b).

The Dulong deposit, located on the southern margin of the Laojunshan granite (Fig. 1b), contains five ore blocks: Tongjie, Manjiazhai, Lazizhai, Nandangchang, and Wukoudong (from north to south) (Fig. 1c). At Dulong, sedimentary rocks are dominated by the Cambrian Xinzhai Formation (main ore host) and Middle Cambrian Tianpeng Formation, which are separated by the northsouth-trending F_2 fault. The Xinzhai Formation is composed of quartz-mica schist, marble, granulite, and minor gneiss. The overlying Tianpeng Formation comprises marble and phyllite and is exposed only in the western Dulong. Three sets of faults were identified at Dulong: NW-trending Maguan-Dulong fault, northsouth (NS) trending ore-controlling faults (F_0, F_1, and F_2), and NW-trending strike-slip fault (F_4) (Fig. 1c). The only granitic rocks exposed at the mine are the late quartz porphyry and granite porphyry dike or apophyses, which represent the southernmost extension of the Laojunshan granite. The early-stage two-mica monzogranite was intersected in drill holes at depth (Su et al. 2016). Recent geological and geochemical studies suggested that the Dulong Sn-Zn polymetallic mineralization was closely related to the Laojunshan granitic magmatism, which is best classified as a magmatic-hydrothermal origin (e.g., Wang et al. 2014; He et al. 2014, 2015; Xu et al. 2015; Ye et al. 2016, 2017, 2018; Zhao et al. 2018).

In the Laojunshan orefield, both the Nanyangtian and Saxi W-Be deposits are located on the eastern side of the Laojunshan granite and share similar ore geological features. The Be mineralization mainly occurred as beryl in the Proterozoic Mengdong Group that is composed by gneiss, schist, and granulite with plagioclase amphibolite interlayers. The beryl crystals are coarse-grained euhedral, some reaching gemstone quality (Liu et al. 2011). The Maka W(-Be) deposit is located in the northern part of the Laojunshan intrusion. The area has different rock types and complex structures, with the Early Paleozoic Maka granitic intrusion being the main magmatic rock type. At Maka, exposed stratigraphy includes mainly the Lower Cambrian Xinzhai Formation and Middle Cambrian Tianpeng Formation, and Be minerals (helvine) coexist with W-bearing minerals (Du et al. 2014).

Sampling and analytical methods

Helvine-group samples of this study were collected from the Sn-Zn polymetallic orebody in the Manjiazhai ore block (Fig. 1c). The Be mineral samples were prepared into 200 μm thick polished thin-sections for the subsequent SEM-BSE and EPMA analyses.

Identification of mineral types and features was mainly performed through laser Raman spectroscopic and scanning electron microscopic (SEM) analyses. EPMA major element mapping analysis, together with LA-ICP-MS trace element analysis, was carried out. To constrain the Be mineralization age, LA-ICP-MS U-Pb dating was conducted on the cassiterite grains in the helvine minerals and their coexisting sphalerite. All the above-mentioned analyses were conducted at the State Key Laboratory of Ore Deposit Geochemistry (SKLODG), Institute of Geochemistry, Chinese Academy of Sciences.

Laser Raman spectroscopy

The analysis was conducted with a Renishaw via Reflex confocal laser Raman spectrometer (U.K.). The analysis used Ar^+ laser, 532 nm wavelength, 50× magnification, 1 μm laser beam size, 514 nm spectroscopic resolution, and 200–1100 cm^{-1} spectroscopic range.

XRD

The powder XRD analysis used a Empyream XRD diffractometer (Netherland). Experimental setting and conditions are Cu*K*α radiation, 40 kV voltage, 40 mA current, 15–95° scan range (2θ), 10(°)/min scan speed, and 0.026° step size.

SEM

The analysis used a JSM-7800F Field Emission SEM (Japan), coupled with a EDAX TEAM Apollo XL energy-dispersive spectroscopy (EDS) and the latest TAEM software version (U.K.). The SEM-EDS can perform fast and accurate qualitative/semi-quantitative determination of mineral phases and their distribution, together with line and planar scanning.

EPMA

The analysis used a JXA8530F-plus Field Emission EPMA (JEOL, Japan). The secondary electron image resolution can reach 3 nm (30 kV, working distance 11 mm), with the spatial resolution better than 0.1 μm. Analytical conditions are 25 kV accelerating voltage, 1.0×10^{-8} A current, 10 μm electron beam size. Since there is no corresponding helvine-group mineral standard, we used almandine (to calibrate FeO, MgO), pyrope (to calibrate TiO_2, Cr_2O_3, Al_2O_3), johannsenite (to calibrate MnO, SiO_2), barite (to calibrate SO_3), willemite (to calibrate ZnO) as standards. The lowest detection limit for the elements analyzed is 0.01%, and the relative error is ±2%. Considering that EPMA direct measurement of Be is still technically difficult (Zhang et al. 2020), the Be contents in helvine are commonly calculated by assuming the stoichiometric ratios of Be with other elements. Previous studies suggested various ways of calculation: (1) helvine-group minerals ideal formula ΣM:Be = 4:3 calculation (Dunn 1976); (2) 12(Al+Be+Si) calculation (Hassan and Grundy 1985; Ragu 1994); (3) 4(Mn+Fe+Zn) calculation (Langhof et al. 2000); (4) 26 (O+S) calculation (Deer et al. 2004; Zito and Hanson 2017); (5) 3Si and 3Be calculation (Raade 2020). Through a detailed comparison analysis of published calculation results, Raade (2020) considered that the assumption of Si = 3 and Be = 3 can effectively avoid the problem of M-site cation substitution by other trace elements in the helvine-group minerals, and yield more accurate and reasonable results. This calculation method, therefore, is used in this study.

LA-ICP-MS trace-element analysis

Trace element analysis used a Coherent 193 nm laser ablation system coupled with an Agilent 7900× ICP-MS. Multiple external standards of USGS reference glass (NIST 610, NIST612, BCR-2G, BIR-1G, BHVO-2G, CGSG-1, analyzed with 44 μm beam size) were used for the calibration and quantitative elemental content calculation (Liu et al. 2008). Recommended elemental contents of the USGS glass are from the GeoReM database (http://georem.mpch-mainz.gwdg.de/). Offline processing of the obtained data, including sample and blank signal selection, instrumental drift calibration, and elemental contents calculation, was performed with the ICPMSDataCal software (Liu et al. 2010).

LA-ICP-MS U-Pb dating

The analysis used the same equipment as the mineral trace-element analysis. Analysis conditions are 60 μm laser beam size, 4 J/cm^2 energy frequency, and 6 Hz

repetitive frequency. To increase sensitivity, helium was used as a carrier gas to mix with the Ar make-up gas before entering the ICP. In-house standard AY-4 was used, and the detailed analysis procedure has been described by Zhang et al. (2017). Offline processing of raw data and the calculation of U-Th-Pb isotope ratios and age were performed with the ICPMSDataCal software (Liu et al. 2010).

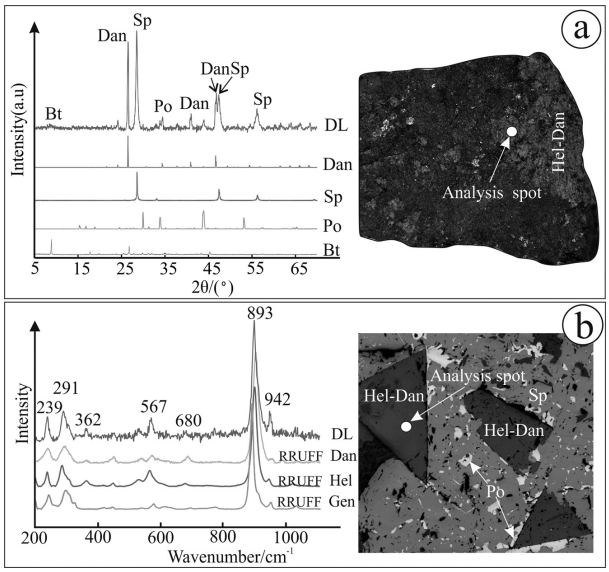

Figure 2. XRD (**a**) and Raman (**b**) images of helvine-group minerals from the Dulong Sn-Zn polymetallic deposit. Abbreviations: Dan = danalite; Sp = sphalerite; Po = pyrrhotite; Bt = biotite; DL = samples from Dulong district; RRUFF mineral = RRUFF Raman database (http://rruff.info).

Results

Helvine-danalite assemblage

XRD results are illustrated in Figure 2a, which shows that the Be minerals are danalite, and they coexist with minerals such as sphalerite, biotite, and pyrrhotite. Raman spectroscopy results show that the Be minerals are helvine (Fig. 2b). It is noteworthy that the three end-member minerals of helvine-group have very similar Raman spectral peaks. As a result, although XRD and Raman analyses can identify helvine-group minerals, they cannot distinguish effectively between the three end-member minerals.

In hand specimens, these helvine-group minerals display triangular profile features. They occur in massive sphalerite ores (Figs. 3a–3b) and coexist with minerals such as sphalerite, pyrrhotite, biotite, and talc (Figs. 3c–3d). Besides, pyrrhotite displays exsolution textures in sphalerite. Under the microscope, it is observed that fine-grained cassiterite coexists with sphalerite and helvine (Figs. 3e–3f).

In the BSE images, some Be minerals developed clear oscillatory zoning (Fig. 4a), as shown by darker helvine and brighter danalite zones and (from inside out) helvine → danalite alternating growth zones. Thus, these Be minerals are oscillatory-zoned helvine-danalite (Figs. 4a–4b). Fluorite veinlets or grains are commonly found inside the helvine-group minerals and coexist with sphalerite or pyrrhotite (Fig. 4c). It is noteworthy that the helvine minerals commonly contain some exsolved minerals, including cassiterite, biotite, ilmenite, and apatite (Figs. 4d–4f).

Major element compositions of helvine-danalite

Results of the EPMA analysis and major-element 2D scan (Fig. 5) and line scan (Fig. 6c) are given in Table 1. BSE imag-

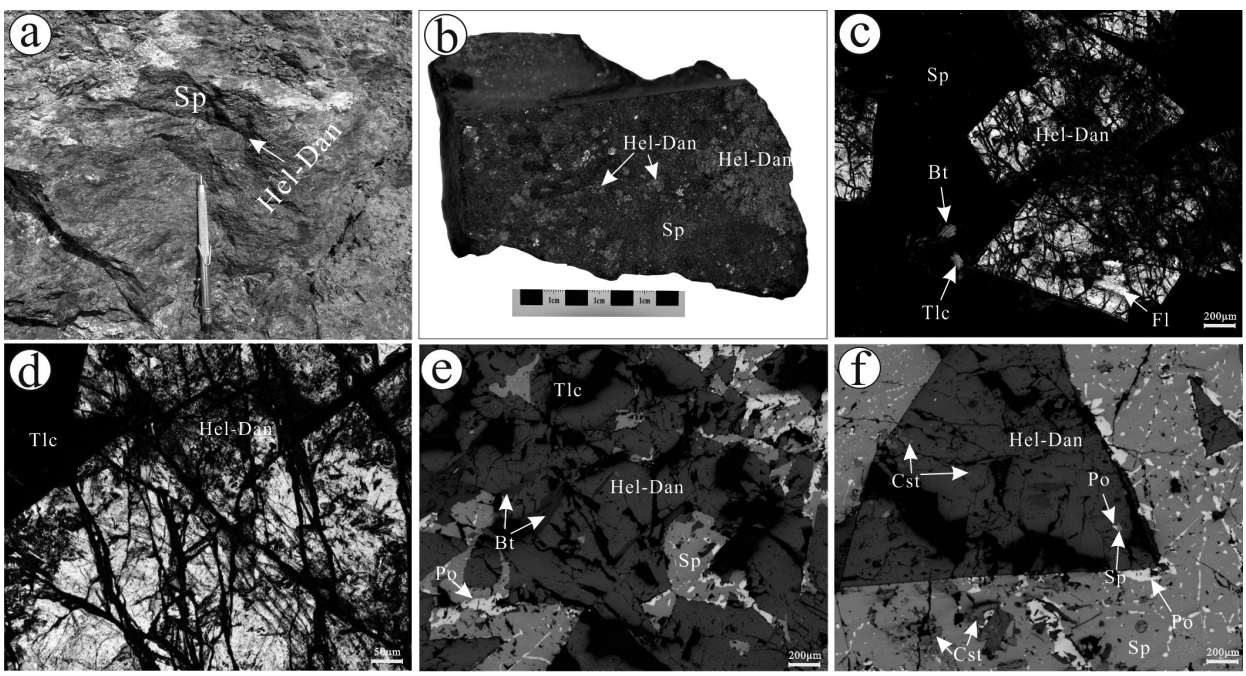

Figure 3. Hand specimen photographs (**a**–**b**); thin-section microphotographs under crossed-polarized light (**c**–**d**) and reflected light (**e**–**f**), showing the intergrowth of sphalerite, Biotite, pyrrhotite, cassiterite, talc and helvine-group minerals. Definitions of mineral abbreviations: Dan = danalite; Hel = helvine; Sp = sphalerite; Po = pyrrhotite; Bt = biotite; Tlc = talc. Cst = cassiterite.

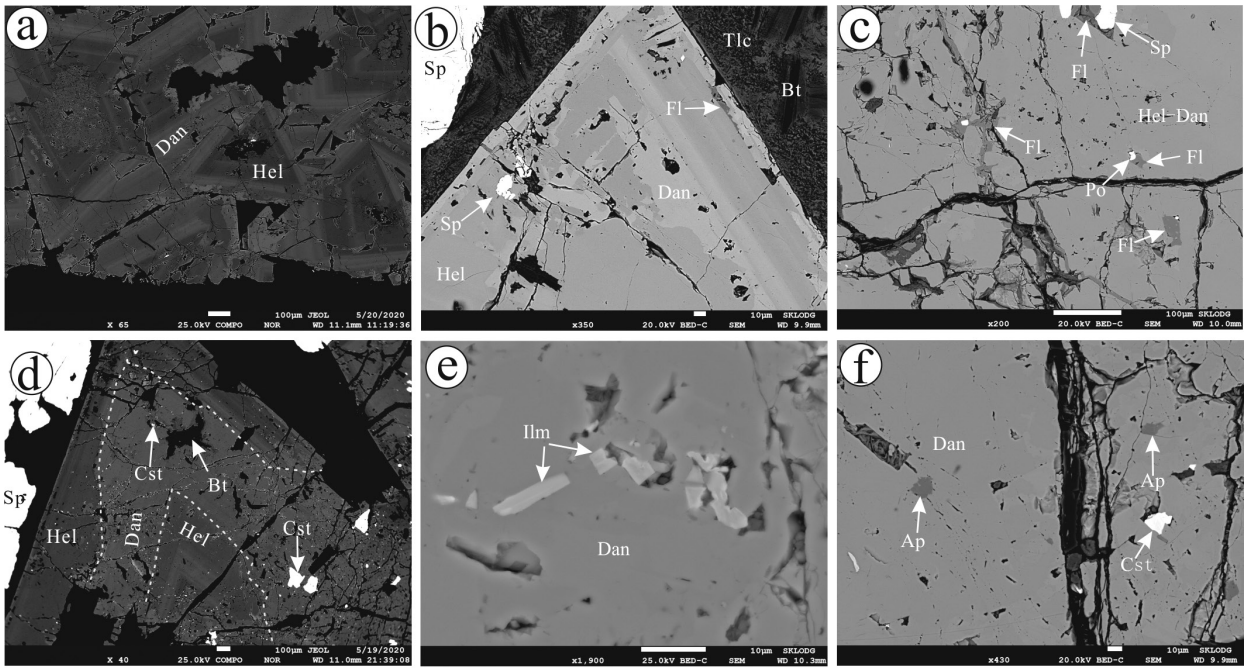

Figure 4. Backscattered electron (BSE) images of helvine-group minerals from Dulong: (**a**–**b**) an euhedral-subhedral oscillatory-zoned helvine-danalite grain, showing intergrowth of sphalerite, talc, biotite, and helvine-danalite. In general, the dark-gray and bright zones are helvine and danalite, respectively; (**c**) fluorite veins or grains intergrown with sphalerite and pyrrhotite in the helvine-danalite; (**d**–**f**) cassiterite, biotite, ilmenite, and apatite in the danalite zone. Abbreviations: Ilm = ilmenite; Ap = apatite, and as in Figure 3.

Table 1. Major element compositions of helvine-danalite

Locality	Core	A	b	c	d	e	f
sample	*n* = 5	*n* = 5	*n* = 5	*n* = 5	*n* = 5	*n* = 5	*n* = 5
Na_2O(wt%)	0.13	0.10	0.14	0.19	0.05	0.05	0.07
MgO	0.05	0.03	0.12	0.07	0.32	0.05	0.29
Al_2O_3	0.20	0.20	0.05	0.13	0.01	0.10	0.01
SiO_2	32.78	32.63	32.64	32.67	32.73	32.89	32.75
CaO	0.27	0.25	0.07	0.20	0.00	0.13	0.06
MnO	37.25	38.54	22.87	29.96	11.74	38.70	8.38
FeO	10.97	9.91	23.73	17.14	30.38	9.74	33.68
ZnO	1.71	1.58	3.83	2.85	9.38	1.72	9.21
S	5.77	5.80	5.77	5.83	5.88	5.71	5.82
O≡S	−2.88	−2.90	−2.88	−2.91	−2.93	−2.85	−2.91
BeO[a]	13.66	13.59	13.60	13.61	13.64	13.70	13.65
Total	99.91	99.74	99.94	99.76	101.22	99.97	101.01
			Cations				
Na (apfu)	0.02	0.02	0.02	0.03	0.01	0.01	0.01
Mg	0.01	0.00	0.02	0.01	0.04	0.01	0.04
Al	0.02	0.02	0.01	0.01	0.00	0.01	0.00
Si	3.00	3.00	3.00	3.00	3.00	3.00	3.00
Ca	0.03	0.02	0.01	0.02	0.00	0.01	0.01
Mn	2.88	3.00	1.78	2.33	0.91	2.98	0.65
Fe	0.84	0.76	1.82	1.31	2.32	0.74	2.57
Zn	0.12	0.11	0.26	0.19	0.64	0.12	0.62
Σ*M*	3.83	3.86	3.86	3.83	3.87	3.84	3.84
S	0.99	1.00	0.99	1.00	1.01	0.98	1.00
Be	3.00	3.00	3.00	3.00	3.00	3.00	3.00
Ternary mol%							
Helvine	75.15	77.56	46.08	60.70	23.52	77.70	16.87
Danalite	21.82	19.66	47.16	34.24	60.01	19.28	66.88
Genthelvite	3.03	2.79	6.76	5.06	16.47	3.02	16.25

Notes: *n* = number of spots. [a] BeO calculated assuming Si = 3 and Be = 3.

ing and EPMA results show that the helvine-danalite grains have many zones from core to rim, with each zone having different chemical compositions (mainly in Mn, Fe, and Zn) (Figs. 5 and 6a): MnO = 8.38–38.70 wt%, FeO = 9.91–33.68 wt%, and ZnO = 1.58–9.21 wt%. In contrast, the Si, S, and **BeO contents have similar ranges: SiO_2 = 32.63–32.89 wt%, S = 5.71–5.85 wt%, **BeO = 13.59–13.70 wt%. Content variations of Mn, Fe, and Zn across the adjacent zone are relatively large, and the variation trend for Fe and Zn is the opposite of that for Mn (Fig. 5). Helvine-group minerals include the end-member minerals of helvine [$Mn_4(BeSiO_4)_3S$], danalite [$Fe_4(BeSiO_4)_3S$], and genthelvite [$Zn_4(BeSiO_4)_3S$]. From the mineral core to rim, no genthelvite is identified in any zone, and inside the helvine and danalite there are varying amounts of the other two end-members (Figs. 6b–6c). Geochemically, the Al and Mg contents are relatively low, and they show covariation patterns with Mn, Fe, and Zn (Fig. 6d).

Trace element compositions of helvine-danalite

For the helvine and danalite zones in the helvine-danalite minerals, their representative LA-ICP-MS trace element and REE data are illustrated in Figure 7 to 8 and Table 2, respectively. Concentrations of some elements (K, Mg, Al, P, Ca, Sc, Y, and Sn) in the helvine-danalite samples are rather high (tens to thousands parts per million), whereas those of some other elements (Na, V, Cu, Rb, Sr, Zr, Nb, Ag, In, Cs, and W) range from below the detection limit to several tens of part per million. The helvine zones have relatively high Al (481–1483 ppm), Ca (650–2573 ppm), Sc (82–133 ppm), and Y (566–1277 ppm), while the danalite zones have relatively high Mg (1425–2337 ppm), P (1151–1551 ppm), and Sn (652–1326 ppm). The samples show chondrite-normalized HREE enrichments, distinct negative Eu anomalies, and relatively high-Y contents (218–1278 ppm) (Fig. 8; Table 2).

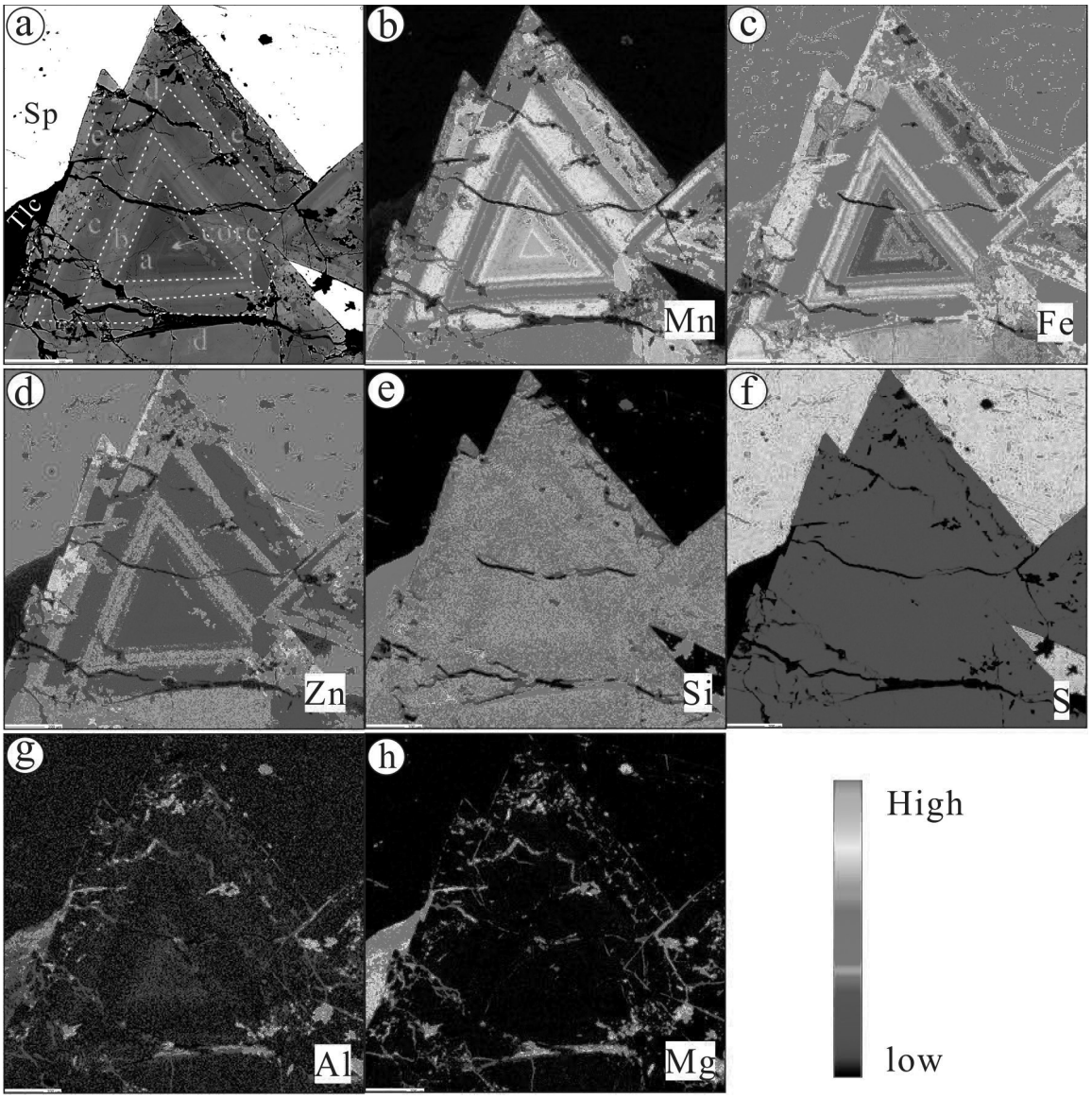

Figure 5. Coupled BSE images with EPMA multi-element maps of the helvine-danalite samples: (**a**) BSE image; (**b**–**h**) EPMA maps of Mn, Fe, Zn, Si, S, Al, and Mg.

Cassiterite U-Pb age

Cassiterite grains in the helvine-danalite and its coexisting sphalerite are relatively large (diameter 10–400 μm) and euhedral (Figs. 3f, 4d, and 9a). As shown in CL images (Fig. 9b), the cassiterite (in sphalerite) grains show clear alternating bright-dark zoning from core to rim. The cassiterite grains have U contents of 0.20–18.36 ppm (Table 3) and yielded a U-Pb lower-intercept concordia age of 86.5 ± 1.6 Ma (2δ, n = 25, MSWD = 1) (Fig. 10).

Discussion

Formation of oscillatory zoning in helvine-danalite

Oscillatory zoning is common in hydrothermal minerals (e.g., garnet, helvine) (Allegre et al. 1981; Wang and Merino 1992; Jamtveit et al. 1993; Shore and Fowler 1996; Zito and Hanson 2017; Antao and Salvador 2019; Raade 2020). Many previous studies proposed two mechanisms for the formation of oscillatory zoning in hydrothermal minerals: (1) internal crystal growth that involves spontaneous chemical self-organization controlled by kinetic factors, such as the mineral growth rate and the diffusion rate of key mineral-forming elements in the fluid (e.g., Allegre et al. 1981; Wang and Merino 1992); (2) periodic fluctuations of external factors, including pressure-temperature (P-T), f_{O_2}, f_{S_2}, and fluid composition during the crystal growth (e.g., Burt 1988; Jamtveit et al. 1993; Raade 2020).

Elemental self-organization of helvine-group minerals. At the Dulong, the chemical compositions of the helvine-danalite oscillatory zoning vary widely (Figs. 6–7; Table 1).

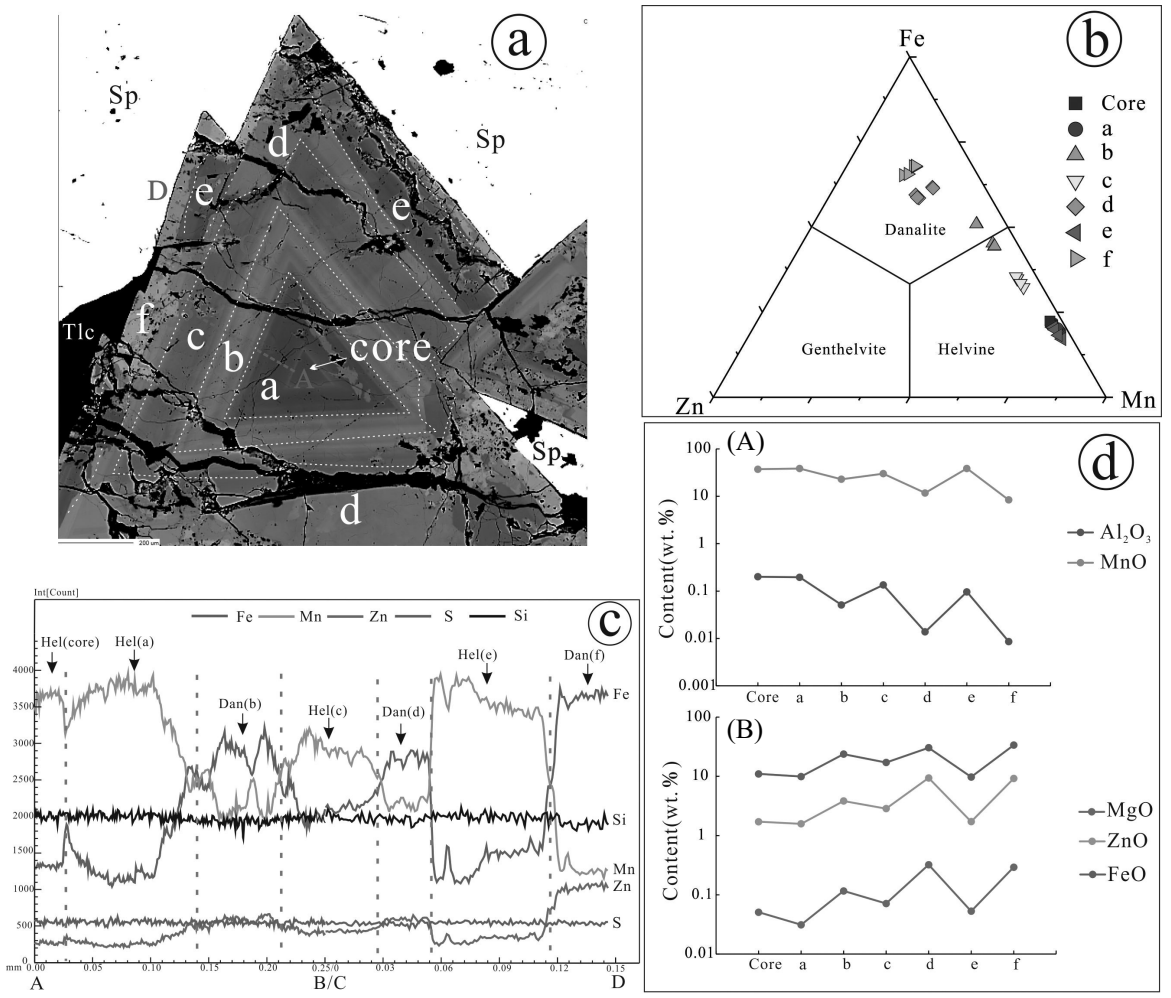

Figure 6. (**a**) BSE image of a helvine-danalite grain, showing seven (core-f) zones in the grain; (**b**) chemical compositions of the seven zones; (**c**) EPMA line scan of Fe, Mn, Zn, S, and Si for profiles A–B and C–D in **a**; (**d**) (A) Correlation diagram of MnO vs. Al_2O_3, (B) (ZnO, FeO) vs. MgO.

In general, the helvine zones contain much higher Mn, K, Al, Ca, Sc, and Y contents but much lower Fe, Zn, Mg, P, and Sn contents than the danalite zones. The Al, Mg, Mn, Zn, and Fe contents vary across different zones, locally up to two orders of magnitude (Fig. 6), and thus achieving that via chemical self-organization is highly unlikely (Kohn 2004).

Hydrothermal fluid composition. Some authors consider that for the formation of genthelvite-helvine zoning (and other complex zoning), the cation availability (notably Mn, Fe, and Zn) in the fluid is highly important (e.g., Raade 2020). However, our helvine-danalite samples occur mainly in massive sphalerite ores, and the sphalerite shows significant pyrrhotite exsolution (Figs. 3e–3f). This implies that neither Zn nor Fe was lacking in the helvine-forming fluid. Genthelvite minerals are absent from core to rim in the helvine-danalite, suggesting that fluctuations of the fluid Mn, Fe, and Zn contents were unlikely to be the main cause for the helvine oscillatory zoning. Meanwhile, previous studies on the helvine oscillatory zoning show no fixed growth sequence from core to rim, e.g., Mn → Fe → Zn (e.g., Dunn 1976; Haapala and Ojanpera 1972; Langhof et al. 2000; Zito and Hanson 2017), Zn → Fe → Mn (e.g., Clark and Fejer 1976), Fe → Zn (e.g., Kwak and Jackson 1986), or Zn → Mn (e.g., Perez et al. 1990; Raade 2020). This further supports that elemental composition in the hydrothermal fluid has probably played little role in the formation of oscillatory zoning in helvine-group minerals.

Sulfur fugacity. Considering the decreasing chalcophilicity of Zn ≥ Fe > Mn, sphalerite would form preferentially instead of genthelvite under high-f_{S_2} conditions, and thus genthelvite is mainly formed in low-f_{S_2} environment (Burt 1980). Helvine and danalite are unstable under low-f_{S_2} conditions, and thus their formation requires relatively high f_{S_2}, under which genthelvite would break down into sphalerite, phenakite, and quartz (Burt 1988). Therefore, the genthelvite formation is highly sensitive to the fluid f_{S_2}. Zinc content (genthelvite mol%) fluctuations may reflect f_{S_2} variation: lower Zn content in the helvine zone (cf. danalite zone) reflects higher f_{S_2}, which is also indicated by the high coexisting sulfide (sphalerite) content in the for-

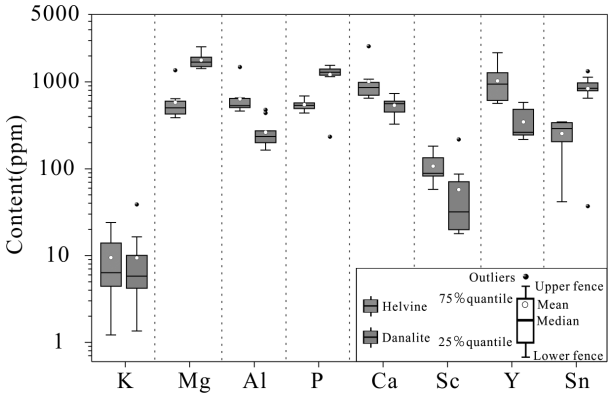

FIGURE 7. Trace element compositions of helvine-group minerals from the Dulong ore district.

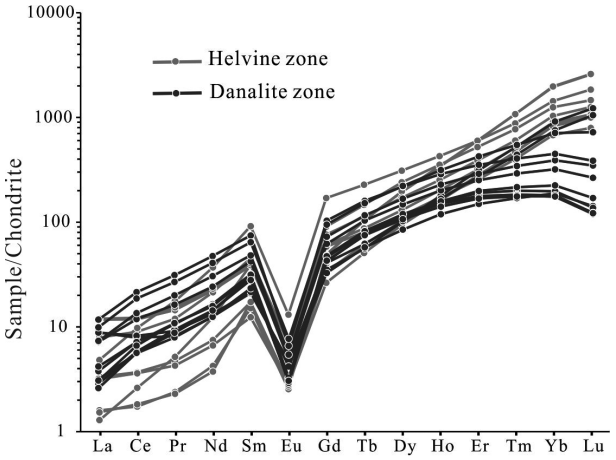

FIGURE 8. Chondrite-normalized REE diagram for the Dulong helvine-group minerals. The chondrite normalizing values are from Taylor and McLennan (1995).

mer (Fig. 4b). At Dulong, the presence of coexisting helvine-danalite with sphalerite and the absence of genthelvite thus indicate a high-f_{S_2} metallogenic environment. From core to rim in the Be mineral samples (Fig. 6a), their Zn contents vary across different zones (Fig. 6c). Overall, three pluses in the Zn content were observed. In the first two pluses, the Zn contents increase first and then decrease, indicating that the f_{S_2} increases first and then drops. In the last pulse, the Zn contents increase continuously, suggesting rising f_{S_2} in the rim during the Be mineral formation.

Oxygen fugacity. Apart from f_{S_2}, the stability of danalite is also highly sensitive to f_{O_2}, and the mineral is stable only in a very narrow f_{O_2} range between fayalite (low f_{O_2}) and hematite-magnetite (high f_{O_2}) (Nimis et al. 1996; Burt 1980). SEM imaging indicates the coexistence of cassiterite and ilmenite in the danalite zones (Figs. 4d–4f), a phenomenon that is absent in the helvine zone. The presence of these oxides implies that danalite is formed in a higher f_{O_2} environment. Therefore, during the oscillatory zoning formation from core to rim (Fig. 6c), the helvine → danalite transition may signify a fluid f_{O_2} rise, while the formation of internal zones danalite → helvine (Fig. 6c) likely suggests a fluid f_{O_2} drop.

In conclusion, helvine-group minerals are unique in the way that they are not purely sulfides or purely silicates, and thus the coupled influence f_{S_2} and f_{O_2} can reasonably explain the zoning formation. As mentioned above, we considered that the Dulong helvine zones were formed under higher f_{S_2} and lower f_{O_2} conditions than the danalite zones. Periodic and coupled fluctuations of the fluid f_{S_2} and f_{O_2} may have led to the formation of the distinct oscillatory zoning observed in the helvine-danalite, in agreement with the conclusion of Raade (2020).

Occurrence and substitution mechanism of trace elements in helvine-danalite

The limited available studies suggest that helvine-group minerals are commonly rich in Ca, Al, Sn, Sc, and Y (e.g., Raimbault and Bilal 1993; Zito and Hanson 2017; Raade 2020). LA-ICP-MS data show that the helvine-group minerals from Dulong contain relatively high contents of Mg, Al, P, Ca, Y, Sc, Sn (from several hundred parts per million to thousand parts per million) and REE (from several parts per million to hundreds of parts per million), and their concentrations vary distinctly in the

TABLE 2. Trace element compositions of helvine-danalite (ppm)

	Mg	Al	P	K	Ca	Sc	Y	Sn	La	Ce	Pr	Nd	Sm	Eu	Gd	Tb	Dy	Ho	Er	Tm	Yb	Lu
Helvine-1	390	553	493	–	827	82.7	689	306	3.64	9.56	1.76	13.4	7.47	0.43	15.6	4.13	41.8	14.4	66.5	16.7	187	34.4
Helvine-2	426	507	549	–	706	92.6	612	323	1.03	2.98	0.58	4.48	3.36	0.21	8.68	2.89	33.0	11.8	58.1	15.1	177	34.1
Helvine-3	467	645	568	–	965	182	1277	348	0.49	1.40	0.29	2.54	2.94	0.19	12.6	5.00	62.4	24.3	125	34.8	407	82.8
Helvine-4	459	654	575	–	989	182	1279	344	0.47	1.47	0.28	2.25	3.37	0.20	12.5	4.89	63.3	24.5	126	34.8	413	83.6
Helvine-5	541	581	439	–	1076	84.8	848	205	2.45	7.27	1.46	12.8	8.83	0.51	19.6	5.34	55.1	18.1	81.1	19.4	216	40.4
Helvine-6	603	518	639	–	898	112	1176	87	1.50	7.90	2.15	22.2	17.8	0.96	44.0	10.8	99.8	30.7	125	28.4	299	59.4
Helvine-7	387	481	523	–	698	57.8	1046	42	0.40	2.11	0.63	7.36	7.59	0.42	23.4	6.92	77.2	25.3	109	25.0	261	47.0
Helvine-8	1364	1483	692	4.63	2574	134	2174	272	21.4	76.2	15.4	124	66.1	4.21	119	25.3	210	59.7	222	44.1	420	76.7
Helvine-9	540	462	467	–	742	64.8	566	274	3.70	9.88	1.87	13.9	7.92	0.40	15.1	3.79	36.9	12.3	53.2	12.9	142	25.5
Helvine-10	643	513	528	–	650	82.7	593	340	0.99	2.91	0.52	3.99	2.40	0.21	6.81	2.40	30.3	11.4	56.8	15.0	172	32.1
Danalite-1	1690	477	1234	196	326	87.0	582	37.0	2.71	6.32	0.98	7.43	4.07	0.33	9.04	2.64	32.6	12.9	65.6	17.1	190	39.3
Danalite-2	1490	221	1321	38.0	516	50.1	339	891	2.21	9.48	1.97	14.4	8.17	0.35	16.0	4.88	47.3	14.4	52.7	9.41	66.5	8.51
Danalite-3	2550	438	1200	36.6	629	28.0	218	652	0.97	4.46	0.96	7.43	4.51	0.30	8.42	2.70	27.2	8.51	31.2	5.47	39.1	4.55
Danalite-4	1926	267	1309	14.8	566	18.4	263	838	0.88	4.63	1.13	8.55	5.63	0.22	10.8	3.58	37.0	11.2	39.8	6.44	41.1	4.39
Danalite-5	1425	166	1268	–	490	19.9	249	843	1.16	5.74	1.28	9.81	6.15	0.21	12.3	3.88	37.9	10.9	37.2	5.90	37.5	3.93
Danalite-6	1500	200	1222	19.8	579	17.9	245	793	1.28	5.72	1.31	9.53	5.80	0.23	11.9	3.72	35.4	10.7	36.6	5.80	36.3	3.82
Danalite-7	1706	235	1407	84.2	562	31.9	263	979	0.94	5.28	1.31	9.39	6.08	0.24	12.1	3.85	38.2	11.3	41.5	6.96	46.6	5.44
Danalite-8	1755	207	1487	6.82	603	70.9	397	1134	2.25	10.8	2.42	18.2	9.32	0.39	18.6	5.47	53.6	16.3	60.5	11.1	81.2	11.1
Danalite-9	1591	250	1293	29.5	449	69.6	483	897	3.61	17.2	3.77	28.2	14.5	0.48	26.6	7.53	70.2	20.6	73.8	13.1	93.6	12.4
Danalite-10	1644	164	1152	–	451	21.1	231	843	0.80	4.51	1.06	8.52	5.42	0.22	11.0	3.53	34.2	10.0	35.1	5.67	36.6	3.90
Danalite-11	2337	273	1552	–	738	218	552	1326	3.04	14.9	3.25	24.3	12.4	0.56	24.4	7.16	71.1	22.4	88.9	17.7	148	23.2

Note: – means under the detection limit.

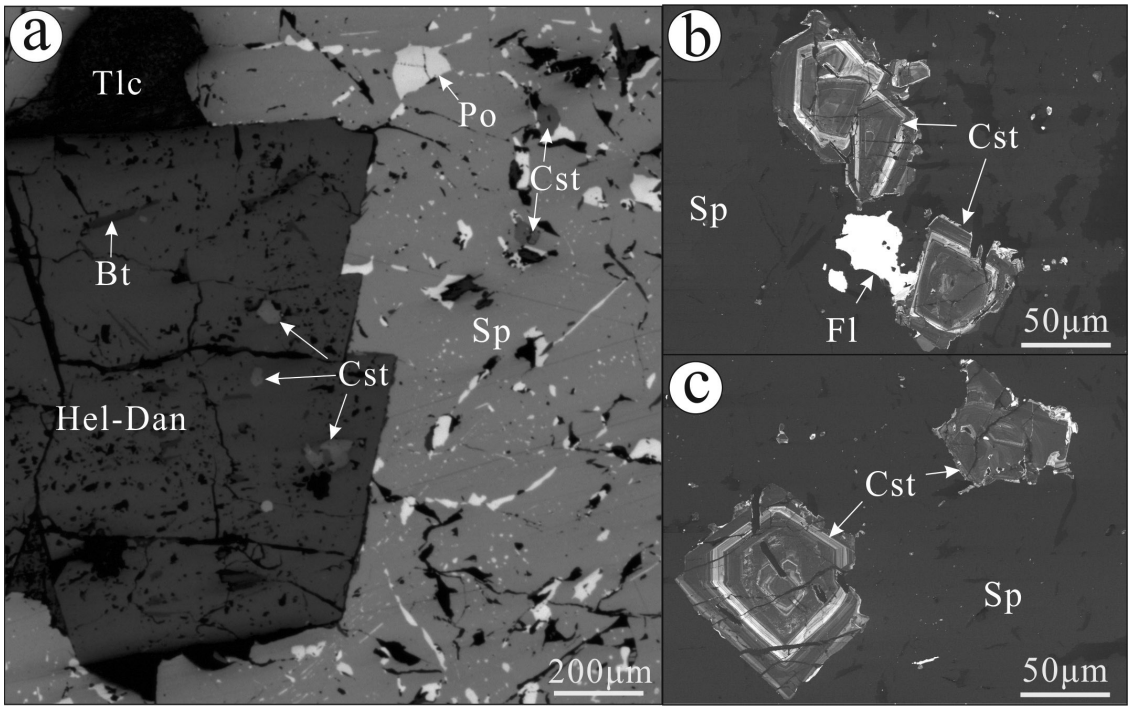

Figure 9. Representative cathodoluminescence (CL) images of the cassiterite intergrown with sphalerite and helvine-group minerals.

helvine and danalite zones (Figs. 7 and 8). The chemical formula of helvine-group minerals can be expressed as $M_4[BeSiO_4]_3S$ and the divalent *M* cation occupies the triangular pyramidic position of the fourfold coordination, while the S atom is positioned at the apex of the pyramid (Hassan and Grundy 1985; Nimis et al. 1996). Compared to the other elements, the difference between the Σ*M* position element and the theoretical value (4 apfu) is the largest, with the former far lower than its theoretical value (Table 1). This indicates that the Σ*M* cation would be easily substituted by other trace elements. EPMA results indicate that the elemental variations between the helvine and danalite zones are only shown in the compositional difference at the Σ*M* position. The Si, **Be, and S compositions are rather fixed, and the differences in elemental features (e.g., ionic radius, chalcophile) at the *M* position may have been the main control for the trace elemental compositions, a viewpoint consistent with many previous studies (Raimbault and Bilal 1993; Zito and Hanson 2017; Raade 2020). The atomic radii and chalcophilicity indices of the major elements and (main)

Table 3. LA-ICP-MS U-Pb dating results of cassiterite from the Dulong tin-zinc polymetallic deposit

Spots	Common Pb	Total Pb	^{232}Th	^{238}U	Isotopic ratios						Isotopic age (Ma)	
	(ppm)	(ppm)	(ppm)	(ppm)	^{207}Pb/^{206}Pb	1σ	^{207}Pb/^{235}U	1σ	^{206}Pb/^{238}U	1σ	^{206}Pb/^{238}U	1σ
DL741	0.13	0.24	0.03	18.36	0.03569	0.00340	0.05985	0.00509	0.01317	0.00031	84.4	2.0
DL74-2	0.16	0.00	0.00	0.27	0.02537	0.00960	0.49927	0.09788	0.01738	0.00222	111	14.1
DL74-3	0.00	0.13	0.00	10.14	0.04241	0.00624	0.06987	0.00883	0.01254	0.00047	80.3	3.0
DL74-4	0.09	0.15	0.00	11.31	0.03666	0.00400	0.06343	0.00575	0.01352	0.00037	86.6	2.3
DL74-5	0.00	0.16	0.04	10.44	0.08023	0.01006	0.13394	0.01482	0.01393	0.00048	89.2	3.1
DL74-6	0.16	0.18	0.03	13.10	0.04754	0.00449	0.08203	0.00661	0.01325	0.00029	84.8	1.8
DL74-7	0.28	0.02	0.00	0.88	0.08124	0.01933	0.27456	0.05713	0.01598	0.00132	102	8.4
DL74-8	0.40	0.20	0.05	14.20	0.04677	0.00538	0.08059	0.00824	0.01345	0.00038	86.1	2.4
DL74-9	0.13	0.01	0.00	0.81	0.08087	0.01815	0.22557	0.03523	0.01482	0.00118	94.8	7.5
DL74-10	0.16	0.05	0.00	2.32	0.11549	0.02015	0.15919	0.01816	0.01558	0.00080	99.6	5.1
DL74-11	0.19	0.21	0.01	8.66	0.13627	0.01028	0.28645	0.01715	0.01652	0.00047	106	3.0
DL74-12	0.11	0.13	0.02	5.17	0.12906	0.01325	0.27687	0.02562	0.01688	0.00064	108	4.1
DL74-13	0.43	0.16	0.02	5.54	0.15082	0.01726	0.30155	0.02038	0.01749	0.00051	112	3.2
DL74-14	0.11	0.10	0.02	4.90	0.12520	0.01550	0.22407	0.01938	0.01511	0.00056	96.7	3.6
DL74-15	0.26	0.11	0.01	3.92	0.20544	0.02705	0.32296	0.02749	0.01659	0.00065	106	4.1
DL74-16	0.15	0.12	0.01	6.33	0.10164	0.01016	0.17451	0.01384	0.01455	0.00051	93.1	3.3
DL74-17	0.00	0.05	0.01	2.25	0.13674	0.01737	0.24638	0.02237	0.01534	0.00083	98.1	5.2
DL74-18	0.13	0.28	0.07	15.05	0.08556	0.00858	0.16329	0.01463	0.01412	0.00046	90.4	2.9
DL74-19	0.21	0.17	0.02	4.74	0.18050	0.01539	0.39962	0.02615	0.01881	0.00070	120	4.4
DL74-20	0.31	0.04	0.02	2.73	0.05885	0.01548	0.08272	0.01535	0.01412	0.00091	90.4	5.8
DL74-21	0.72	0.37	0.02	7.11	0.23255	0.01461	0.68060	0.03474	0.02359	0.00073	150	4.6
DL74-22	0.37	0.01	0.00	0.66	0.05627	0.01506	0.19074	0.03857	0.01513	0.00132	96.8	8.4
DL74-23	0.18	0.01	0.00	0.20	0.02620	0.01152	0.51409	0.11291	0.02124	0.00383	135	24.2
DL74-24	0.00	0.02	0.03	0.96	0.14262	0.02802	0.39899	0.05537	0.01665	0.00114	106	7.2
DL74-25	0.43	0.21	0.00	15.28	0.03955	0.00581	0.06027	0.00682	0.01353	0.00044	86.6	2.8

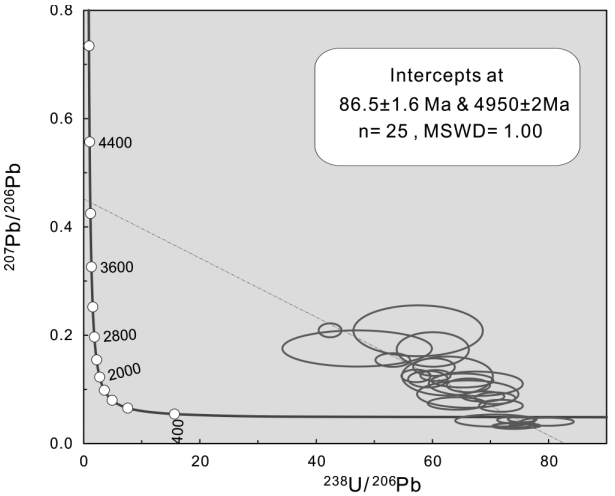

Figure 10. Tera-Wasserburg U-Pb age diagrams for the cassiterite from the Dulong ore district.

trace elements measured are shown in Figure 11.

K, Ca, and P. Under fourfold coordination, the ionic radii of K^+ (1.27 Å) and P^{5+} (0.17 Å) are rather different from those of Mn^{2+} (0.80 Å), Fe^{2+} (0.63 Å), and Zn^{2+} (0.60 Å) in the *M* position (Fig. 11), which makes substitution unlikely from an ionic radius perspective. Although no Ca^{2+} ionic radius data (under fourfold coordination) were given by Shannon (1976), the Ca^{2+} ionic radius (under sixfold coordination: 1 Å) is still rather different from that of Mn^{2+}, Fe^{2+}, and Zn^{2+} (under sixfold coordination), which means that Ca^{2+} does not easily enter the helvine structure. Meanwhile, BSE imaging shows that helvine-danalite contains significant amounts of K-, Ca-, and P-rich minerals, such as biotite, apatite, and fluorite (Figs. 4c, 4d, and 4f). Therefore, we consider that the K, Ca, and P occur mainly as micro-inclusions in the helvine-danalite matrix.

Al and Mg. In view of the similar ionic radius among Mg^{2+}, Fe^{2+}, and Zn^{2+} under fourfold coordination (Fig. 11) and the good positive Mg vs. (Fe+Zn) correlation (Figs. 6d), we consider Mg substitutes readily Zn and Fe at the *M* position. Under fourfold coordination, the ionic radius of Al^{3+} is rather different from that of the M-site cations, and its chalcophilicity is also not similar

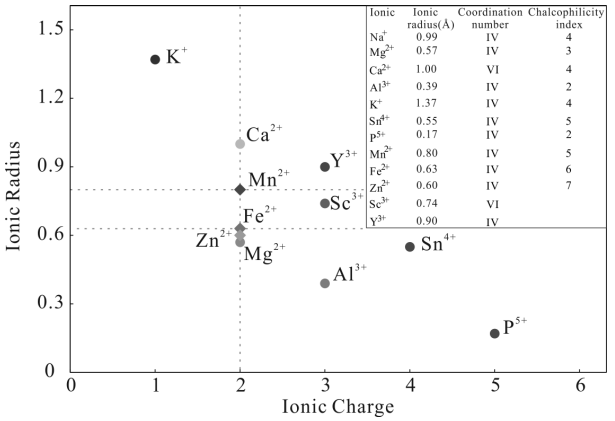

Figure 11. Plot of ionic charge vs. ionic radius (fourfold coordination except Ca^{2+} and Sc^{3+}; from Shannon 1976) and chalcophilicity index (Christy 2018) for the elements measured.

(Fig. 11). EPMA results show that the contents of Al are well correlated with those of Mn (Fig. 6d), suggesting that Al can be incorporated into the helvine-group minerals by substituting Mn. This indicates that trace element distributions in the helvine-group minerals are influenced by the atomic size, elemental chalcophilicity, and external factors including the fluid f_{S_2}, f_{O_2}, and crystal structure. The trivalent cation (e.g., Al^{3+}) entering the tetrahedron position is required in the coupled substitution to maintain the charge neutrality of the crystal structure (e.g., Smith et al. 2004; Gaspar et al. 2008). At Dulong, both the helvine and danalite zones contain relatively high-total (Σ) REE contents (up to 1500 ppm). The fact that Al has good linear relations with *M* position elements and REE indicates that the helvine-group minerals may have coupled substitution mechanism of Al and REEs: $Al^{3+} + REE^{3+} + \square = 3M^{2+}$ (Fig. 12a)

Sn, Sc, and Y. Radde (2020) considered that although Sn^{2+} has higher chalcophilicity than Sn^{4+}, the Sn in helvine-group minerals is more likely to be Sn^{4+} from a stereochemical perspective. Under fourfold coordination, the ionic radius of Sn^{4+} is similar to those of Zn^{2+} and Fe^{2+} but different from that of Mn^{2+} (Fig. 11). Therefore, Sn substitutes readily the Zn and Fe at the *M* position [$Sn^{4+} + \square = 2(Fe,Zn)^{2+}$]. This is supported by the much higher content of Sn in danalite compared with that in helvine (Fig. 7), consistent with the results of Radde (2020). Many studies have reported high-Sc contents in helvine-group minerals (Raimbault and Bilal 1993; Zito and Hanson 2017; Raade 2020). For instance, Radde (2020) reported that the Sc_2O_3 in helvine can reach 1.53 wt% and argued that Sc substitutes into the *M* position via $2Sc^{3+} + \square = 3(Mn,Fe,Zn)^{2+}$. The Dulong helvine-danalite samples have also relatively high-Sc content (up to 100 ppm), with that in the helvine zone higher than that in the danalite zone (Fig. 7). Although no Sc^{3+} ionic radius data (under fourfold coordination) were given by Shannon (1976), elemental chalcophilicity behavior analysis suggests that Sc is a strongly lithophile element and is thus similar to Mn from a chalcophilicity perspective (Christy 2018). This could explain the relatively high-Mn content in helvine, although the possible influence from Sc-bearing mineral micro-inclusions in helvine cannot be excluded. Compared with the reported Y contents in helvine-group minerals (Zito and Hanson 2017), the helvine-danalite from Dulong have anomalously high-Y contents (up to 1200 ppm), with the helvine zones being especially rich Y (Fig. 7). Under fourfold coordination, Y^{3+} has more similar ionic radius to Mn^{2+} than that of Zn^{2+} and Fe^{2+}. From an ionic radius perspective, therefore, Y can readily substitute Mn in the M-site cations, which is consistent with the high-Y content measured in the Dulong helvine. Therefore, Y may enter the M-site cations via $2Y^{3+} + \square = 3Mn^{2+}$.

In conclusion, K, P, and Ca occur mainly in helvine-group minerals as micro-inclusions, while Mg, Sn, Y, and Sc can enter readily into the M-sites of helvine-group minerals through isomorphic substitution of Mn, Fe, and Zn. Coupled substitution between Al and REEs can also occur in these minerals.

REE in helvine-danalite

Since Y and REE^{3+} have very similar geochemical behavior in hydrothermal minerals (e.g., garnet), if the entry of these elements into garnet is only controlled by crystal-chemical factors (e.g., coupled substitution mechanism), REE^{3+} contents would be

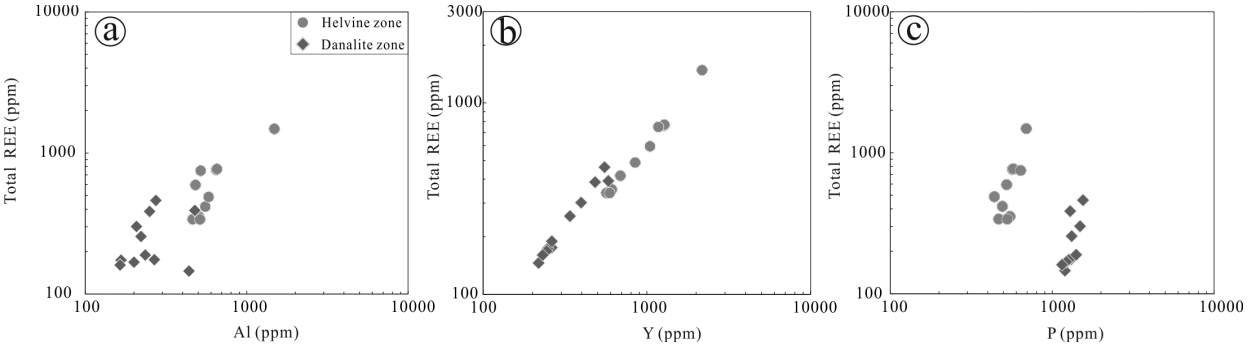

Figure 12. Trace element and REE diagrams of helvine-group minerals in the Dulong ore district.

strongly related to Y (Dziggel et al. 2009; Park et al. 2017). This phenomenon is also found in our helvine-danalite samples (Fig. 12b). Thus, the Dulong helvine-danalite has similar coupled substitution behavior for REEs and Y to that in hydrothermal garnet: $REE^{3+} + Y^{3+} \rightarrow 3(Mn,Fe,Zn)^{2+}$.

HREE-enrichments in helvine were reported in many previous studies (Raimbault and Bilal 1993; Zito and Hanson 2017). However, the HREE-enrichment mechanism in helvine remains unclear. For example, Raimbault and Bilal (1993) considered that the HREE-enrichment in helvine may have been crystallographically controlled, similar to the REE geochemical behavior in garnet (REEs substitute readily major elements of Fe, Mn, and Zn). Zito and Hanson (2017) considered that the HREE-enrichments in helvine are related to F-rich fluid, as supported by thermodynamic calculation models. Equilibrium constant of the HREE-F complexes is higher than that of the LREE-F complexes, and thus F complexes preferentially with HREEs and forms the HREE enrichments in helvine-group minerals (Gramaccioli et al. 1999; Gramaccioli and Pezzotta 2000). Previous REE analyses on helvine-group minerals did not systemically analyze Y or P (Raimbault and Bilal 1993; Zito and Hanson 2017), and hence the influence of these element on REE-enrichment is poorly constrained. Our results indicate that the Dulong helvine-danalite contains high contents of HREEs, Y, and P, and these elements show good mutual linear relations (Figs. 12b and 12c). Meanwhile, helvine commonly precipitates under relatively alkaline conditions (Perez et al. 1990; Finch 1990; Burt 1977, 1980), and fluorine and phosphate ions can effectively complex with REEs (especially HREEs) (Mineyev 1963; Sillen and Martell 1964; Dumonceau et al. 1979). Hence, we attribute HREE enrichments in the Dulong helvine-danalite to F-Y(-P) enrichments in the ore fluids.

It is noteworthy that the Dulong helvine-danalite samples show distinct negative Eu anomalies in chondrite-normalized REE distribution patterns. Previous studies indicate that the Eu decoupling (expressed as positive or negative anomalies) in REEs requires valence changes of Eu, which in turn requires changes in the fluid redox conditions. Fluid redox conditions are commonly co-influenced by the fluid temperature-pressure, f_{O_2}, pH, and chemical compositions (Bau 1991; Wood 1990; Slack et al. 2000), and the main control for the type of REE occurrence is temperature (Sverjensky 1984; Bau 1991). Theoretical calculation indicates that when the temperature is >250 °C, Eu occurs mainly as Eu^{2+} (Sverjensky 1984). Previous fluid inclusion microthermometric studies on the sulfide-coexisting minerals from Dulong (fluorite, dolomite, quartz, and calcite) yielded ore-formation temperatures of 204–398 °C (Ye et al. 2016), under which Eu in the fluid should occur mainly as Eu^{2+}. Therefore, during the helvine-group minerals precipitation at Dulong, the fluid Eu may have mainly occurred as Eu^{2+}. The reduction of Eu^{3+} to Eu^{2+} is accompanied by an increase in ionic radius and the decrease of adsorption capacity of Eu^{2+} (compared to other REEs) on the helvine-danalite mineral surface, which eventually generates the observed negative Eu anomalies.

Regional Be mineralization potential in the Laojunshan orefield

The Be minerals in the Laojunshan orefield comprise mainly oscillatory-zoned helvine-danalite, with its coexisting cassiterite U-Pb dated to be 86.5 ± 1.6 Ma. The age is consistent (within error) with the reported cassiterite U-Pb ages (87.2 ± 3.9 Ma to 89 ± 1.4 Ma) in the orefield (Wang et al. 2014; Zhao et al. 2018). Published mineralization ages from Dulong (Fig. 13; Liu et al. 2007, 2011; Li et al. 2013; Wang et al. 2014; Xu et al. 2015; Zhao et al. 2018) indicate that both the Be and Sn mineralization are coeval with and likely resulted from the Laojunshan granite intrusion and its associated hydrothermal activities (Liu et al. 2007; Wang et al. 2014; Xu et al. 2015; Zhao et al. 2018). Notably, many Be deposits/prospects have been discovered in the Laojunshan orefield, e.g., the Nanyangtian W deposit and Saxi W-Be (mainly beryl) deposits in the SE Laojunshan orefield, and the Maka W(-Be) (mainly helvine) deposit in the northern Laojunshan orefield. This suggests that the Be mineralization occurred in a regional scale. Recently reported ages for the orefield include high-precision biotite ^{40}Ar-^{39}Ar isochron ages (Nanyangtian: 97.01 ± 1.39 Ma and 99.58 ± 0.98 Ma; Wang et al. 2019), biotite ^{40}Ar-^{39}Ar inverse isochron age (Saxi and Maka: 119 ± 3 Ma; Liu 2011), and zircon U-Pb ages (Maka: 415.6 ± 1.8 Ma, 411.2 ± 3.5 Ma, 400.7 ± 3.0 Ma) of the ore-causative intrusion (Du et al. 2014). These age data imply that the Be mineralization at Dulong, Nanyangtian, and Saxi all occurred in the Cretaceous (Fig. 13), during which the Laojunshan pluton was emplaced. At Maka, the ore-related intrusion is largely coeval (within error) to the Silurian Nanwenhe granitic gneiss (Liu et al. 2006). As the Nanwenhe granitic gneiss is widespread in the Laojunshan orefield, whether there was an older Early Paleozoic Be mineralization episode in the orefield needs further investigations.

In the southern end of the Laojunshan intrusion (Su et al. 2016), the presence of high-K calc-alkaline and highly fractionated S-type granite (Liu et al. 2007; Lan et al. 2016; Xu et al. 2015;

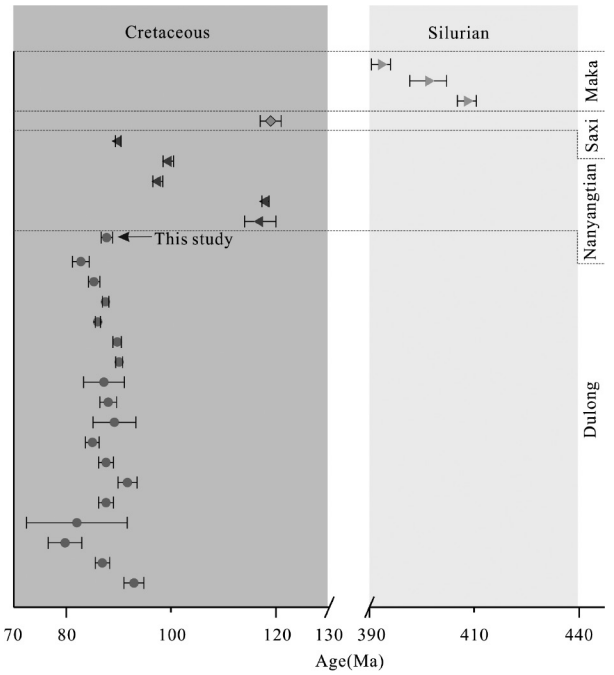

Figure 13. Age range of representative granites and associated Be deposits in the Laojunshan orefield (modified after Liu et al. 2007, 2011; Li et al. 2013; Wang et al. 2014, 2019; Du et al. 2014; Xu et al. 2015; Zhao et al. 2018).

Zhao et al. 2018) implies that the high-Na and K assemblage would preferentially form phenakite and feldspars (instead of beryl) and that the Al would form feldspathoids. This is consistent with previous suggestions that alkali granite-related Be mineralization would form helvine-group minerals instead of beryl (Perez et al. 1990; Finch 1990; Burt 1977, 1980). We, therefore, suggest that the entire orefield may have substantial Be mineralization potential, which may partly explain why beryl is not found around the Laojunshan intrusion.

Implications

Helvine-group minerals have been identified at Dulong Sn-Zn deposits, SE Yunnan. They comprise oscillatory-zoned helvine and danalite, which transition generally (from core to rim) from helvine to danalite but with multiple alternating growths in between. The well-developed oscillatory zoning is likely attributed to the periodic f_{O_2} and f_{S_2} fluctuations during the mineral formation and is less related to the fluid compositional variation.

The helvine-danalite from Dulong contains high contents of trace elements (including mainly Ca, Mg, Al, Sc, Sn, Y, and REEs). The Ca, K, and P may have occurred mainly as micro-inclusions in the helvine-danalite, while the Sn, Sc, and Y likely enter the helvine (*M* position) via isomorphic substitution. Affected by the ionic radius, elemental chalcophilicity, and physicochemical conditions, the Sc and Y preferentially enter helvine and Sn and Mg into danalite.

The helvine-danalite samples are featured by HREE enrichments and negative Eu anomalies, with the ΣREE of helvine distinctly higher than danalite. This may be caused by the higher Y and P in the helvine and higher F in the fluid. F-Y-rich fluid and phosphate ion would preferentially complex HREEs and enter helvine. REE minerals mainly enter helvine through $Y^{3+} + REE^{3+} + \square = 3(Mn,Fe,Zn)^{2+}$, as well as through coupled substitution of Al with REEs. The dominance of Eu^{2+} for Eu in the fluid may have generated the observed negative Eu anomalies.

The helvine-coexisting cassiterite from Dulong is U-Pb dated to be 86.5 ± 1.6 Ma, coeval with the Dulong Sn-Zn polymetallic mineralization. This implies that both are products of the Cretaceous Laojunshan magmatic-hydrothermal activity. Regional mineralization age compilation indicates that Cretaceous (plus possibly Early Paleozoic) Be mineralization is common in the orefield, and the whole orefield has likely substantial potential for Be discovery.

Acknowledgments and Funding

We thank the Editor Hongwu Xu, Associate Editor Matthew Steele-Maclnnis, and two anonymous reviewers for their comments on our manuscript, and appreciate the assistance of Yunfeng Liu, Suoqing Zhang, and Qinfu Ye from the Yunan Hualian Zinc and Indium Stock Co. Ltd. in South Yunnan province and Hang Su from Yunnan Hualian Mineral Exploration Co. Ltd. during our fieldwork. We acknowledge Yanwen Tang and Junjie Han from the State Key Laboratory of Ore Deposit Geochemistry (SKLODG), Institute of Geochemistry, Chinese Academy of Sciences (IGCAS) for their assistance in performing the experiments. This study was funded by the National Key R&D Program of China (2016YFC0600503).

References cited

Allegre, C.J., Provost, A., and Jaupart, C. (1981) Oscillatory zoning: A pathological case of crystal growth. Nature, 294, 223–228.

Antao, S.M., and Salvador, J.J. (2019) Crystal chemistry of birefringent uvarovite solid solutions. Minerals, 9, 395.

Bau, M. (1991) Rare-earth element mobility during hydrothermal and metamorphic fluid-rock interaction and the significance of the oxidation state of europium. Chemical Geology, 93, 219–230.

Burt, D.M. (1977) Chalcophile-lithophile tendencies in the helvite group: genthelvite stability in the system $ZnO–BeO–Al_2O_3–SiO_2–SO_{-1}–F_2O_{-1}$ (abstract). American Geophysical Union Transactions, 58, 1242.

——— (1980) The stability of danalite, $Fe_4Be_3(SiO_4)_3S$. American Mineralogist, 65, 355–360.

——— (1988) Stability of genthelvite, $Zn_4(BeSiO_4)_3S$: An exercise in chalcophilicity using exchange operators. American Mineralogist, 73, 1384–1394.

Christy, A.G. (2018) Quantifying lithophilicity, chalcophilicity and siderophilicity. European Journal of Mineralogy, 30, 193–204.

Clark, A.M., and Fejer, E.E. (1976) Zoned genthelvite from the Cairngorm Mountains, Scotland. Mineralogical Magazine, 40, 637–639.

Deer, W.A., Howie, R.A., Wise, W.S., and Zussman, J. (2004) Rock-forming Minerals, Vol. 4B, Framework silicates. Second ed. The Geological Society of London, 352–368.

Du, S.J., Wen, H.J., Qing, C.J., Yan, Y.F., Yang, G.S., and Feng, P.Y. (2014) Occurrence of beryllium in the Maka Tungsten Polymetallic deposit in Malipo County, Yunnan Province and its significance. Acta Mineralogica Sinica, 34, 446–450 (in Chinese with English abstract).

Dumonceau, J., Bigot, S., Treuil, M., Faucherre, M., and Fromage, F. (1979) Détermination des constantes de formation des tétracarbonatolanthanidates (III). Revue de Chimie Minérale, 16, 583–592.

Dunn, P.J. (1976) Genthelvite and the helvine-group. Mineralogical Magazine, 40, 627–636.

Dziggel, A., Wulff, K., Kolb, J., Meyer, F.M., and Lahaye, Y. (2009) Significance of oscillatory and bell-shaped growth zoning in hydrothermal garnet: Evidence from the Navachab gold deposit. Chemical Geology, 262, 262–276.

Finch, A.A. (1990) Genthelvite and willemite, zinc minerals associated with alkaline magmatism from the Motzfeldt center. Mineralogical Magazine, 54, 407–412.

Gaspar, M., Knaack, C., Meinert, L.D., and Moretti, R. (2008) REE in skarn systems: A LA-ICP-MS study of garnets from the Crown Jewel Deposit. Geochimica et Cosmochimica Acta, 72, 185–205.

Goldschmidt, V.M. (1932) Geochemische Leit-Elemente. Die Naturwissenschaften, 20, 947–948.

Gramaccioli, C.M., and Pezzotta, F. (2000) Geochemistry of yttrium with respect to the rare-earth elements in pegmatites. Memorie Della Italiana di Scienze e Del Museo Civico di Storia Naturale di Milano XXX, 111–115.

Gramaccioli, C.M., Diella, V., and Demartin, F. (1999) The role of fluoride complexes in REE geochemistry and the importance of 4f electrons: some examples in minerals. European Journal of Mineralogy, 11, 983–992.

Grew, E.S., and Hazen, R.M. (2014) Beryllium mineral evolution. American Mineralo-

gist, 99, 999–1021.
Haapala, I., and Ojanpera, P. (1972) Genthelvite-bearing greisens in southern Finland. Bulletin of the Geological Survey of Finland, 259, 22.
Hassan, I., and Grundy, H.D. (1985) The crystal structures of helvite group minerals, $(Mn,Fe,Zn)_8(Be_6Si_6O_{24})S_2$. American Mineralogist, 70, 186–192.
He, F., Zhang, Q., Wang, D.P., Liu, Y.P., Ye, L., and Bao, T. (2014) Ore-forming materials sources of the Dulong Sn-Zn polymetallic deposit, Yunnan, evidences from S-C-O stable isotope. Bulletin of Mineralogy, Petrology and Geochemistry, 33, 900–907 (in Chinese with English abstract).
He, F., Zhang, Q., Liu, Y.P., Ye, L., Miao, Y.L., Wang, D.P., Su, H., Bao, T., and Wang, X.J. (2015) Lead isotope compositions of Dulong Sn-Zn polymetallic deposit, Yunnan, China: Constraints on ore-forming metal sources. Acta Mineralogica Sinica, 35, 32–40 (in Chinese with English abstract).
Jamtveit, B., Wogelius, R.A., and Fraser, D.G. (1993) Zonation patterns of skarn garnets: Records of hydrothermal system evolution. Geology, 21, 113–116.
Kohn, M.J. (2004) Oscillatory- and sector-zoned garnets record cyclic (?) rapid thrusting in central Nepal. Geochemistry, Geophysics, Geosystems, 5.
Kwak, T.A.P., and Jackson, P.G. (1986) The compositional variation and genesis of danalite in Sn–F–W skarns, NW Tasmania, Australia. Neues Jahrbuch für Mineralogie, Monatshefte, 452–462.
Lan, J.B., Liu, Y.P., Ye, L., Zhang, Q., Wang, D.P., and Su, H. (2016) Geochemistry and age spectrum of Late Yanshanian granites from Laojunshan Area, Southeastern Yunnan Province. China. Acta Mineralogica Sinica, 36, 441–454 (in Chinese with English abstract).
Langhof, J., Holtstam, D., and Gustafsson, L. (2000) Chiavennite and zoned genthelvite–helvite as late-stage minerals of the Proterozoic LCT pegmatites at Uto, Stockholm, Sweden. GFF, 122, 207–212.
Li, J.K., Wang, D.H., Li, H.Q., Cheng, Z.H., and Mei, Y.P. (2013) Late Jurassic-early Cretaceous mineralization in the Laojunshan ore concentration area, Yunnan province. Earth Science-Journal of China University of Geosciences, 38, 1023–1036 (in Chinese with English abstract).
Li, J.K., Zou, T.R., Wang, D.H., and Ding, X. (2017) A review of beryllium metallogenic regularity in China. Mineral Deposits, 36, 951–978 (in Chinese with English abstract).
Liu, Y.P., Ye, L., Li, C.Y., Song, B., Li, T.S., Guo, L.G., and Pi, D.H. (2006) Discovery of the Neoproterozoic magmatics in southeastern Yunnan: evidence from SHRIMP zircon U-Pb dating and lithogeochemistry. Acta Petrologica Sinica, 22, 916–926 (in Chinese with English abstract).
Liu, Y.P., Li, Z., Li, H., Guo, L., Xu, W., Ye, F., Li, C., and Pi, D. (2007) U-Pb geochronology of cassiterite and zircon from the Dulong deposit: Evidence for Cretaceous large-scale granitic magmatism and mineralization events in southeastern Yunnan Province, China. Acta Petrologica Sinica, 23, 967–976 (in Chinese with English abstract).
Liu, Y.S., Hu, Z.C., Gao, S., Günther, D., Xu, J., Gao, C.G., and Chen, H.H. (2008) In situ analysis of major and trace elements of anhydrous minerals by LA-ICP-MS without applying an internal standard. Chemical Geology, 257, 34–43.
Liu, Y., Hu, ZChu., Zong, K., Gao, CGui., Gao, S., Xu, J., and Chen, H. (2010) Reappraisement and refinement of zircon U-Pb isotope and trace element analyses by LA-ICP-MS. Chinese Science Bulletin, 55, 1535–1546.
Liu, Y.P., Li, Z.X., Ye, L., Tan, H.Q., and Li, C.Y. (2011) Ar-Ar chronology of tungsten mineralization in Laojunshan ore concentration area. Acta Mineralogica Sinica, 617–618 (in Chinese).
Mineyev, D.A. (1963) Geochemical differentiation of the rare earths. Geochemistry, 1129–1149.
Nimis, P., Molin, G., and Visona, D. (1996) Crystal chemistry of danalite from Daba Shabeli Complex (N Somalia). Mineralogical Magazine, 60, 375–379.
Park, C., Song, Y., Kang, I.M., Shim, J., Chung, D., and Park, C.S. (2017) Metasomatic changes during periodic fluid flux recorded in grandite garnet from the Weondong W skarn deposit. Chemical Geology, 451, 135–153.
Perez, J.B., Dusausoy, Y., Babkine, J., and Pagel, M. (1990) Mn zonation and fluid inclusions in genthelvite from the Taghouaji complex (Air Mountains, Niger). American Mineralogist, 75, 909–914.
Raade, G. (2020) Helvine-group minerals from Norwegian granitic pegmatites and some other granitic rocks: cases of significant Sc and Sn contents. Canadian Mineralogist, 58, 367–379.
Ragu, A. (1994) Helvite from the French Pyrénée as evidence for granite-related hydrothermal activity. Canadian Mineralogist, 32, 111–120.
Raimbault, L., and Bilal, E. (1993) Trace-element contents of helvite-group minerals from metasomatic albitites and hydrothermal veins at Sucuri, Brazil, and Dajishan, China. Canadian Mineralogist, 31, 119–127.
Shannon, R.D. (1976) Revised effective ionic radii and systematic studies of interatomic distances in halides and chalcogenides. Acta Crystallographica, A32, 751–767.
Shore, M., and Fowler, A.D. (1996) Oscillatory zoning in minerals: A common phenomenon. Canadian Mineralogist, 34, 1111–1126.
Sillen, L.G., and Martell, A.E. (1964) Stability constants of metal-ion complexes. London, Chemical Society, Special publication, Royal Society of Chemistry, no. 17.
Slack, J.F., Meier, A.L., Malcolm, M.J., Fey, D.L., Doughten, M.W., and Wanless, G.A. (2000) Trace element and rare-earth element geochemistry of bedded and massive sulfides from the Sullivan Pb-Zn-Ag deposit, British Columbia—A reconnaissance study. In J.W. Lydon, T. Hoy, J.F. Slack, and M.E. Knapp, Eds., The Geological Environment of the Sullivan Pb-Zn-Ag Deposit, British Columbia. Eological Association of Canada, Mineral Deposits Division, Special Publication, vol. 1, p. 720–735.
Smith, M.P., Henderson, P., Jeffries, T.E.R., Long, J., and Williams, C.T. (2004) The rare earth elements and uranium in garnet from the Beinn an Dubhaich aureole, Skye, Scotland, U.K. Journal of Petrology, 45, 457–484.
Su, H., Wei, W.B., Tao, Z.H., Dao, X.Q., and Li, T.J. (2016) Geological and geochemical characteristics of later Yanshanian concealed granite and its relation with Sn-Zn polymetallic mineralization. Acta Mineralogica Sinica, 36, 488–496 (in Chinese with English abstract).
Sverjensky, D.A. (1984) Europium redox equilibria in aqueous solution. Earth and Planetary Science Letters, 67, 70–78.
Taylor, S.R., and McLennan, S.M. (1995) The geochemical evolution of the continental crust. Reviews of Geophysics, 33, 241–265.
Wang, Y.F., and Merino, E. (1992) Dynamic model of oscillatory zoning of trace elements in calcite: Double layer, inhibition, and self-organization. Geochimica et Cosmochimica Acta, 56, 587–596.
Wang, C.Y., Han, R.S., Huang, J.G., Xu, S.H., and Ren, T. (2019) The ^{40}Ar–^{39}Ar dating of biotite in ore veins and zircon U-Pb dating of porphyritic granite dyke in the Nanyangtian tungsten deposit in SE Yunnan, China. Ore Geology Reviews, 114, 103133.
Wang, X.J., Liu, Y.P., Miao, Y.L., Bao, T., Ye, L., and Zhang, Q. (2014) In LA-MC-ICP-MS cassiterite U-Pb dating of Dulong Sn-Zn polymetallic deposit and its significance. Acta Petrologica Sinica, 30, 867–876 (in Chinese with English abstract).
Wood, S.A. (1990) The aqueous geochemistry of the rare-earth elements and yttrium: 2. Theoretical predictions of speciation in hydrothermal solutions to 350 °C at saturation water vapor pressure. Chemical Geology, 88, 99–125.
Xu, B., Jiang, S.Y., Wang, R., Ma, L., Zhao, K.D., and Yan, X. (2015) Late Cretaceous granites from the giant Dulong Sn-polymetallic ore district in Yunnan Province, South China: Geochronology, geochemistry, mineral chemistry and Nd-Hf isotopic compositions. Lithos, 218-219, 54–72.
Yan, D.P., Zhou, M.F., Wang, C.Y., and Xia, B. (2006) Structural and geochronological constraints on the tectonic evolution of the Dulong-Song Chay tectonic dome in Yunnan province, SW China. Journal of Asian Earth Sciences, 28, 332–353.
Ye, L., Bao, T., Liu, Y.P., He, F., Wang, X.J., Zhang, Q., Wang, D.P., and Lan, J.B. (2018) The trace and rare elements in scheelites and their implication for mineralization in Dulong Sn-Zn polymetal ore deposit, Yunnan Province. Journal of Nanjing University (Natural Science), 54, 245–258 (in Chinese with English abstract).
Ye, L., Bao, T., Liu, Y.P., Zhang, Q., Wang, X.J., He, F., Wang, D.P., and Lan, J.B. (2016) Mineralization stages and ore-forming fluid of Dulong Sn-Zn polymetal ore deposit, Yunnan Province, China. Acta Mineralogica Sinica, 36, 503–509 (in Chinese with English abstract).
Ye, L., Liu, Y.P., Zhang, Q., Bao, T., He, F., Wang, X.J., Wang, D.P., and Lan, J.B. (2017) Trace and rare elements characteristics of sphalerite in Dulong super large Sn-Zn polymetallic ore deposit, Yunnan province. Journal of Jilin University, Earth Science Edition, 47, 734–750 (in Chinese with English abstract).
Zhang, R., Lehmann, B., Seltmann, R., Li, C., and Sun, W. (2017) Cassiterite U-Pb geochronology constrains magmatic-hydrothermal evolution in complex evolved granite systems: The classic Erzgebirge tin province (Saxony and Bohemia). Geology, 45, 1095–1098.
Zhang, W.L., Che, X.D., Wang, R.C., Xie, L., Li, X.F., and Zhang, D. (2020) Optimum conditions for quantitative analysis of beryllium by electron probe microanalysis: a case study of beryl. Chinese Science Bulletin, 65, 3205–3216.
Zhao, Z., Hou, L., Ding, J., Zhang, Q., and Wu, S. (2018) A genetic link between Late Cretaceous granitic magmatism and Sn mineralization in the southwestern South China Block: A case study of the Dulong Sn dominant polymetallic deposit. Ore Geology Reviews, 93, 268–289.
Zito, G., and Hanson, S.L. (2017) Genthelvite overgrowths on danalite cores from a Pegmatite Miarolitic Cavity in Cheyenne Canyon, El Paso County, Colorado. Canadian Mineralogist, 55, 195–206.

Manuscript received December 6, 2020
Manuscript accepted July 15, 2021
Manuscript handled by Matthew Steele-MacInnis